NURETH14-585

COMPUTATIONAL FLUID DYNAMIC INVESTIGATIONS OF THERMAL STRATIFICATION IN THE HOT POOL OF MONJU REACTOR AND COMPARISON WITH MEASURED DATA

Juby Abraham, K.Velusamy and P.Chellapandi

Nuclear and Safety Engineering Group
Indira Gandhi Centre for Atomic Research, Kalpakkam – 603 102, India
Juby@igcar.gov.in, kvelu@igcar.gov.in, pcp@igcar.gov.in

Abstract

As a part of IAEA collaborative research project, thermal stratification in MONJU hot pool has been predicted for the event of turbine trip. Predicted temperature distribution has been compared against the data measured in MONJU reactor. It is observed that stratification prevails in the pool for a shorter duration than that observed in the plant. Also, predicted axial temperature gradient at the stratification interface is larger than that measured in the reactor. Predictive capabilities of various turbulence models and the effect of thermal capacity of hot pool structures on stratification have been assessed by parametric studies.

Keywords: Computational fluid dynamics, thermal stratification, turbulence models, validation.

Introduction

In fast reactors with breeder subassemblies and internal storage of spent fuel subassemblies, temperatures of sodium exiting from fuel, breeder and spent subassemblies are vastly different. Due to this temperature difference coupled with large thermal expansion coefficient of sodium and large size of the reactor pool (a few meters), the Richardson number in the pools is of the order of unity, indicating that the inertial and buoyancy forces are of similar magnitudes. As a result of this, a stratification interface where a large temperature change occurs over a short height is developed [1–2]. The stratification interface is unstable with respect to position and it leads to low frequency ($\sim 0.01 - 2$ Hz) temperature oscillations of large amplitude. Since the heat transfer coefficient of sodium is very large, the fluid temperature fluctuations are transmitted to adjoining structures with minimum attenuation. One of the important thermal loads on fast reactor components is axial temperature gradient at the stratification and its fluctuation with respect to time. Thermal stratification in the pool can also develop due to plant transients. Apart from hot pool, thermal stratification can develop in sodium pipelines also, if the conditions are conducive. For the structural design of the components and pipelines, knowledge of steady and transient temperature distributions prevailing in the components is essential. Large-scale sodium experiments to predict thermal stratification are costly and time consuming due to (i) high freezing point of sodium, (ii) opaque nature of sodium and (iii) violent chemical reactor of sodium when exposed to air or water. Normal fluids like air and water cannot simulate sodium conditions for heat transfer, due to large difference in the values of their Prandtl numbers vis-à-vis that of sodium. Hence, CFD prediction of thermal stratification assumes significance in fast reactor design and safety evaluation. Turbulence model is a critical issue in CFD analysis, especially for stratified flow conditions. Most of the turbulence models have been developed mainly for forced convective flows. Identification of suitable turbulence model for buoyancy dominated flows, assessment of predictive capabilities of standard turbulence models for liquid metal applications with stratification and establishing the adequacy of mesh and approximation made in the geometry for small scale structures in the pool are all ongoing research activities in the domain of CFD for fast reactor applications. Transient hot pool temperature distributions, measured in MONJU reactor during the event of reactor trip followed by 'loss of condenser vacuum' can be used as a benchmark data set for the validation of CFD tools, especially for stratified flow conditions. This is the motivation for the coordinated research project initiated by IAEA. MONJU is a loop type sodium cooled Japanese fast reactor. Measurements carried out in the hot pool of MONJU during steady state and simulated transient conditions of turbine trip from 40 % power indicate strong stratification of sodium.

1. Input data

MONJU is a 714 MWt prototype fast breeder reactor with liquid sodium as the primary coolant and 3 secondary sodium loops. Various components and structures in the hot pool are depicted in Figs. 1 and 2 [3-5]. The reactor vessel is a vertical cylindrical vessel with three outlet nozzles, which are provided to transport hot sodium to intermediate heat exchangers. An inner barrel with two rows of holes is kept inside the reactor vessel. The upper core structure (Fig. 2) consists of control plug main body, CRD guide tubes, honeycomb structure, flow guide tubes and thermocouple fingers. A thermocouple rack, which is housing 36 thermocouples for hot pool sodium temperature measurements, is positioned at 305° at a radial distance of 3.043 meter from reactor vessel centre. The reactor core is having 18 flow zones as depicted in Fig. 3.

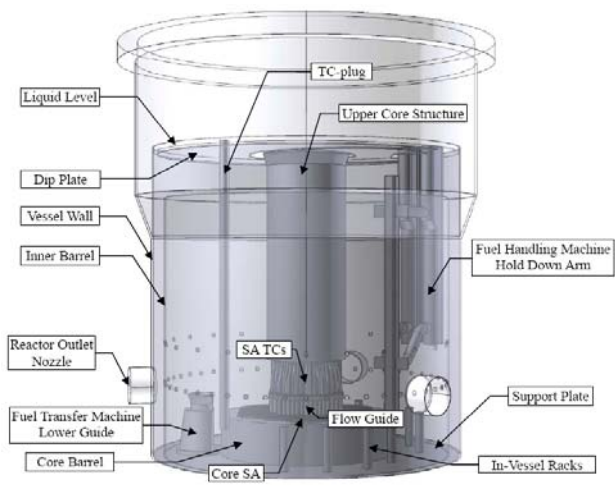


Figure 1 Components and structures in MONJU hot pool



Figure 2 Various parts in the Upper Core Structure of MONJU reactor

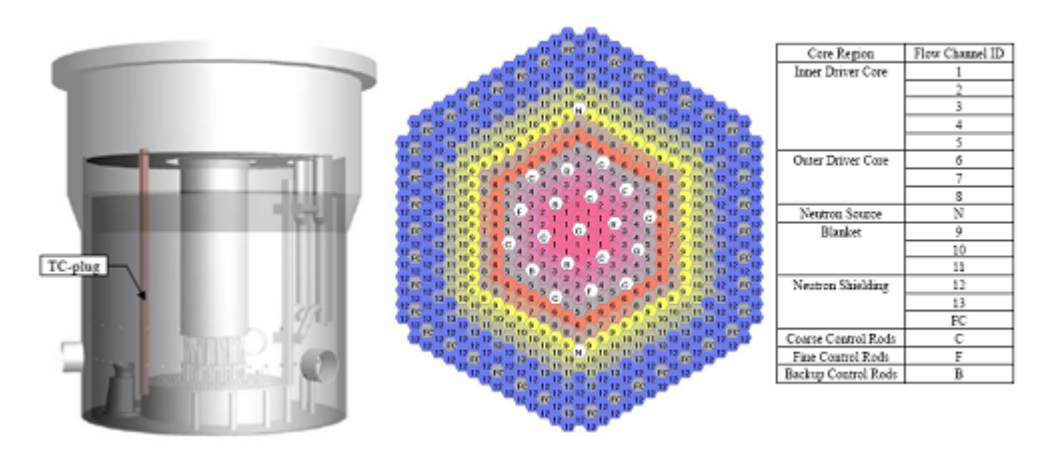


Figure 3 Thermocouple position and Reactor core of MONJU reactor

2. Numerical Simulation

2.1 Computational domain

A 60° segment of the MONJU upper plenum excluding fuel handling and transfer system is considered for the analysis which is depicted in Fig. 4. To maintain symmetry with respect to hexagonal core, outlet nozzle is rotated 12.5° in clockwise direction. Upper core structure and control rod guide tube are represented explicitly in this model. Flow guide tubes, honeycomb grid and fingers are accounted by appropriate porous media models. The flow holes in the inner barrel are also modeled explicitly. Inner barrel is modeled as an adiabatic gap.

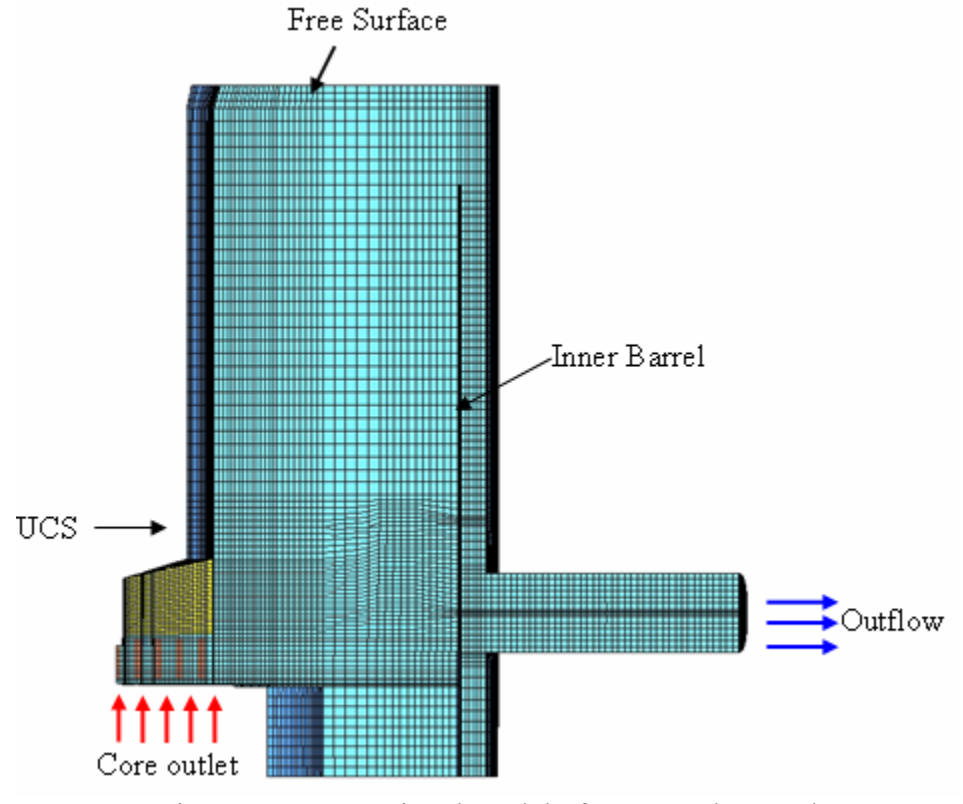


Figure 4 Computational model of MONJU hot pool

Computations have been carried out using the commercial CFD code STAR-CD [6]. Material properties are assumed as constant. About 0.28 million hexahedral mesh have been employed for the simulation.

2.2 Governing equations

The conservation equations for mass, momentum and energy are [7]:

$$\nabla \cdot (\rho \vec{u}) = \frac{\partial \rho}{\partial t} \tag{1}$$

$$\frac{\partial(\rho\vec{v})}{\partial t} + \nabla \cdot (\rho\vec{u}\vec{u}) = -\nabla p + \nabla \cdot \left[\mu \left(\nabla\vec{u} + \nabla\vec{u}^T\right)\right] + \rho\vec{g}$$
 (2)

$$\frac{\partial}{\partial t}(\rho C_P T) + \nabla \cdot \left(\overrightarrow{u} \left(\rho C_P T \right) \right) = \nabla \cdot \left(K_{eff} \nabla T \right)$$
(3)

The fluid is considered as incompressible and to account for buoyancy effects, the Boussinesq approximation is used. The steady state calculation is done by using SIMPLE algorithm with first order upwind schemes for the discretisation of convection terms in all the governing equations. The sum of the residuals in the discretised equations is set to less than 10⁻⁵ for declaring convergence during steady state as well as transient simulations. For transient calculation PISO algorithm is used to resolve the pressure-velocity coupling.

2.3 Turbulence model

Since the flow is turbulent, the high Reynolds number standard k- ε model is considered in the present work for the basic model (benchmark model) as well as for the model with hot pool thermal capacity. For near wall treatment standard wall function is used. The two differential equations that govern the transport of turbulence kinetic energy (k) and its dissipation rate (ε) are given by [8]

$$\frac{\partial}{\partial_{t}} (\rho k) + \frac{\partial}{\partial x_{i}} (\rho k u_{i}) = \frac{\partial}{\partial x_{i}} \left[\left(\mu + \frac{\mu_{t}}{\operatorname{Pr}_{t-k}} \right) \frac{\partial k}{\partial x_{j}} \right] + G_{k} + G_{b} - \rho \varepsilon$$
 (5)

$$\frac{\partial}{\partial_{t}}(\rho\varepsilon) + \frac{\partial}{\partial x_{i}}(\rho\varepsilon u_{i}) = \frac{\partial}{\partial x_{j}} \left[\left(\mu + \frac{\mu_{t}}{\Pr_{t-\varepsilon}} \right) \frac{\partial\varepsilon}{\partial x_{j}} \right] + C_{1\varepsilon} \frac{\varepsilon}{k} \left(G_{k} + C_{3\varepsilon} G_{b} \right) - C_{2\varepsilon} \rho \frac{\varepsilon^{2}}{k}$$
 (6)

In eqns. (5) & (6), G_k is calculated as

$$G_k = -\rho \overline{u_i' u_j'} \frac{\partial u_j}{\partial x_i} \tag{7}$$

and G_b is calculated as:

$$G_b = \beta g_i \frac{\mu_t}{\text{Pr.}} \frac{\partial T}{\partial x_i}$$
 (8)

The turbulent viscosity (μ_t) is computed from k and ε as follows:

$$\mu_t = \rho C_\mu \frac{k^2}{\varepsilon} \tag{9}$$

The model constants are given below:

$$C_{1\varepsilon} = 1.44$$

$$C_{2\varepsilon} = 1.92$$

$$C_{\mu} = 0.09$$

A constant value of 1.44 is used for the model constant, $C_{3\varepsilon}$ as recommended in STAR-CD [6] The turbulent Prandtl numbers for k and ε are 1.0 and 1.3 respectively.

As a variant, the Gibson-Launder Reynolds Stress Turbulence Model [6] has also been adopted, to assess its predictive capacity compared to that of the standard k-ε model.

2.4 Porous body formulation

The flows through the main body and control rod guide tubes of the upper core structure (UCS) are assumed as zero. CEA has analyzed the pressure drop in upper core structure and put forth an equivalent porous body model for this region. Hence, components like flow guide tubes, honeycomb grid and fingers are modeled as porous sub-region as recommended by CEA [9]. Direction dependant pressure loss coefficients are used to account for the resistance offered by fine-scale structures of UCS. The pressure loss coefficient, for flow guide tubes and fingers are calculated from friction factor correlations for pin bundle configurations [9].

As per CEA Report [9],

$$F_p = -\rho C_f \frac{|\vec{v}|}{2D} \vec{v} \tag{10}$$

where,
$$C_f = a \operatorname{Re}^{-b}$$
 and $\operatorname{Re} = \frac{\rho v D}{\mu}$

The values of constants *a* and *b* are dependant on both magnitude and direction of flow and are given in Table 1. The charecterestic velocity and length are also given in Table 1.

b D a Hydraulic Axial direction 0.316 0.25 Axial velocity diameter, D_h Horizontal External Transverse direction 4.03 0.27 velocity Diameter, De

Table 1. Constants for porous media model

In line with these parameters, the inputs for STAR-CD are $\alpha = \frac{\rho C_f}{2D}$ and $\beta = 0$

A porous baffle assumption is made to account for the resistance of honeycomb grid structure. Porous baffle resistance is calculated from

$$\Delta p = \frac{1}{2} \rho K |v_n| v_n \tag{11}$$

The value of K suggested by CEA is 25. Therefore, $\alpha = 12.5$ and $\beta = 0$ have been used.

2.5 Thermal capacity model of UCS

To evaluate the effect of thermal capacity of the structures, thermal structures viz. upper core structure, inner barrel and upper core support plate are modeled. Upper core structure of the reactor is represented by an equivalent heat capacity. The volumetric percentage of stainless steel and sodium are [10]:

Stagnant liquid sodium: 82.1% Stainless steel: 17.9%

The sodium mass exchange between inside and outside of the UCS surface is negligible. Sodium flow from CRD Guide tubes is also considered as negligible. Sodium flow from CRD assemblies into UCS

through the CRD guide tubes is also neglected. Thick bottom support plate, inner barrel and reactor vessel are modeled and their heat capacity is accounted. The guide tubes for FCRs, CCRs and BCRs have only negligible paths for sodium because they are almost plugged above the vertical position of the honeycomb plate by complicated structures of the drive mechanisms. Heat loss through the thermal insulation of reactor vessel wall is also assumed as negligible.

2.6 Boundary and initial condition

The 18 flow regions are fed with velocity and temperature of core outlet flow. For steady state velocities according to 40% power condition is given. During transient period the measured flow and temperature values are given at the outlet of core. Symmetric condition is applied to both faces of sector of hot pool. The walls of inner barrel are considered as adiabatic. The outlet nozzle is extended and thus outflow boundary condition is applied.

3. Results and Discussion

3.1 3-D Benchmark model: steady state

The predicted velocity and temperature distributions in the hot pool at a vertical section through outlet nozzle are depicted in Fig. 5. Sodium from core outlet enters the pool at $\sim 30^{\circ}$ inclination to the horizontal. On meeting the inner barrel, it turns upwards towards free surface. But the flow does not travel up to free surface. It turns out radially at the top of the inner barrel and then passes downwards through the annulus between inner barrel and the reactor vessel, before leaving through the outlet nozzle. There is an anti-clockwise recirculation region near the main body of upper core structure. The velocity of flow through inner barrel holes is of the order of 0.5 m/s only. The sodium between the core barrel and the inner barrel is nearly stagnant, leading to stratification.

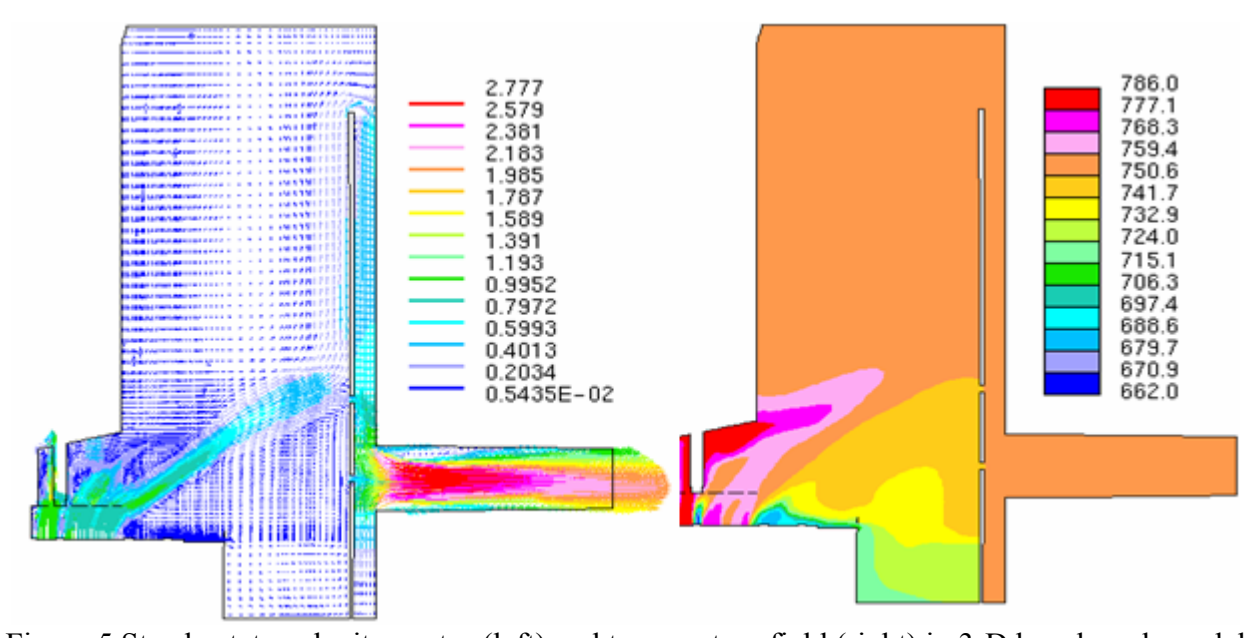


Figure 5 Steady state velocity vector (left) and temperature field (right) in 3-D benchmark model

The cavity between core barrel and the inner barrel is isothermal at ~ 715 K. There is large temperature variation in the axial distance between core top and main body of UCS. Above this, again the pool is isothermal at ~ 755 K.

3.2 3-D Benchmark model: transient

Transient analysis of hot pool simulating the turbine event has been carried out to predict the movement of stratification front with respect to time for a period of 3600s. The predicted velocity and temperature fields in a vertical plane through outlet nozzle at 5 instances are depicted in Figs. 6 and 7 respectively. It is evident that the communication from hot pool to outlet nozzle is primary through the holes in the inner barrel. But, there is still significant flow from hot pool to outlet nozzle via the annulus between inner barrel and reactor vessel, as evident from the temperature contours. The interface moves upwards gradually as time marches. The flow through the holes in the inner barrel increases first and then decreases. As the flow falls the buoyancy flow set in and the fresh cold sodium tries to by-pass through the holes in the inner barrel. But later as the total flow becomes very less, the flow through the holes also reduces.

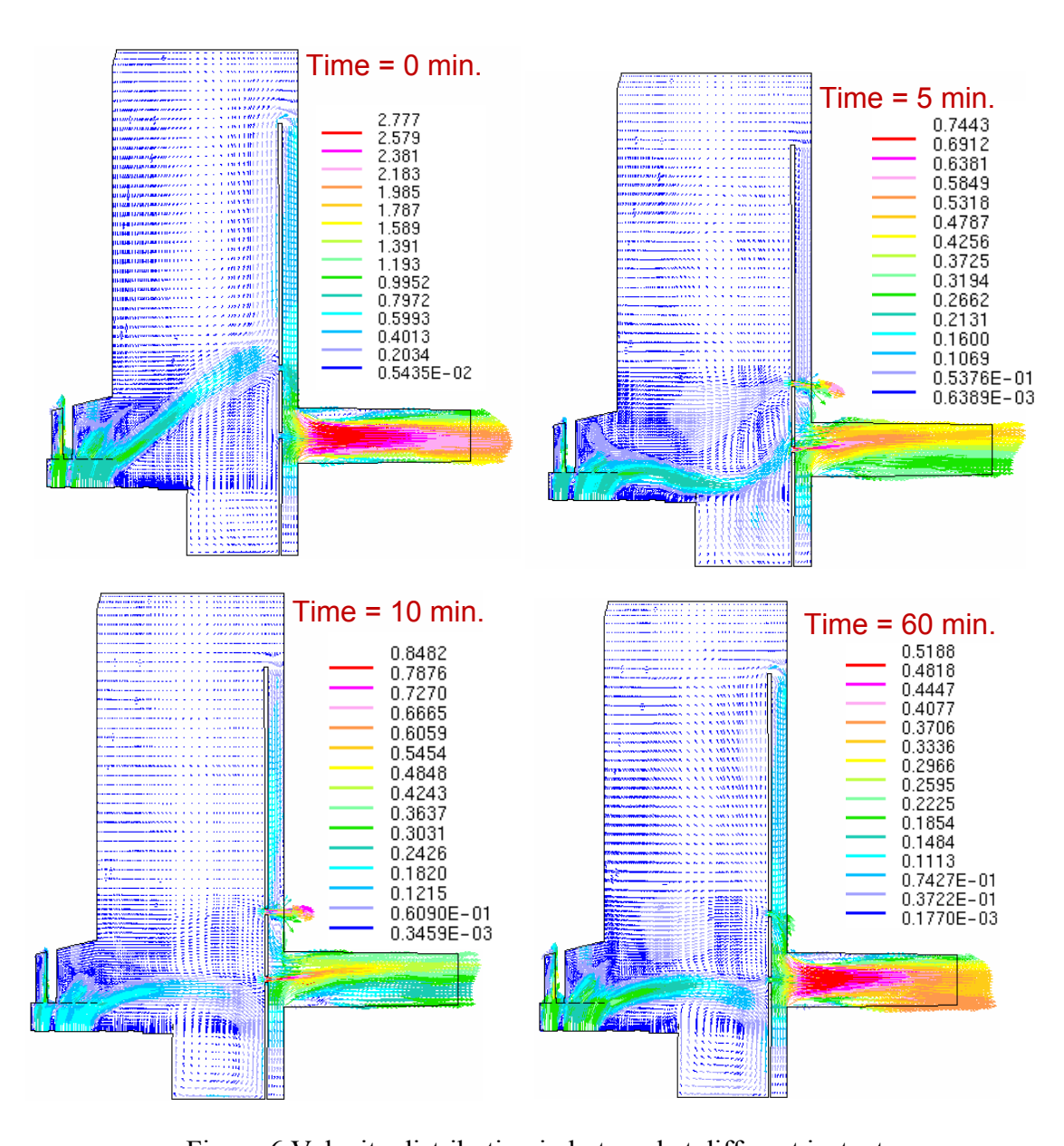


Figure 6 Velocity distribution in hot pool at different instants

3.3 3-D Thermal capacity model: transient

A simulation for duration of 3600s is carried out to predict the effect of thermal capacity on thermal stratification of hot pool. Flow pattern is found to be similar to bench mark model and movement of interface is same as the benchmark model as time marches.

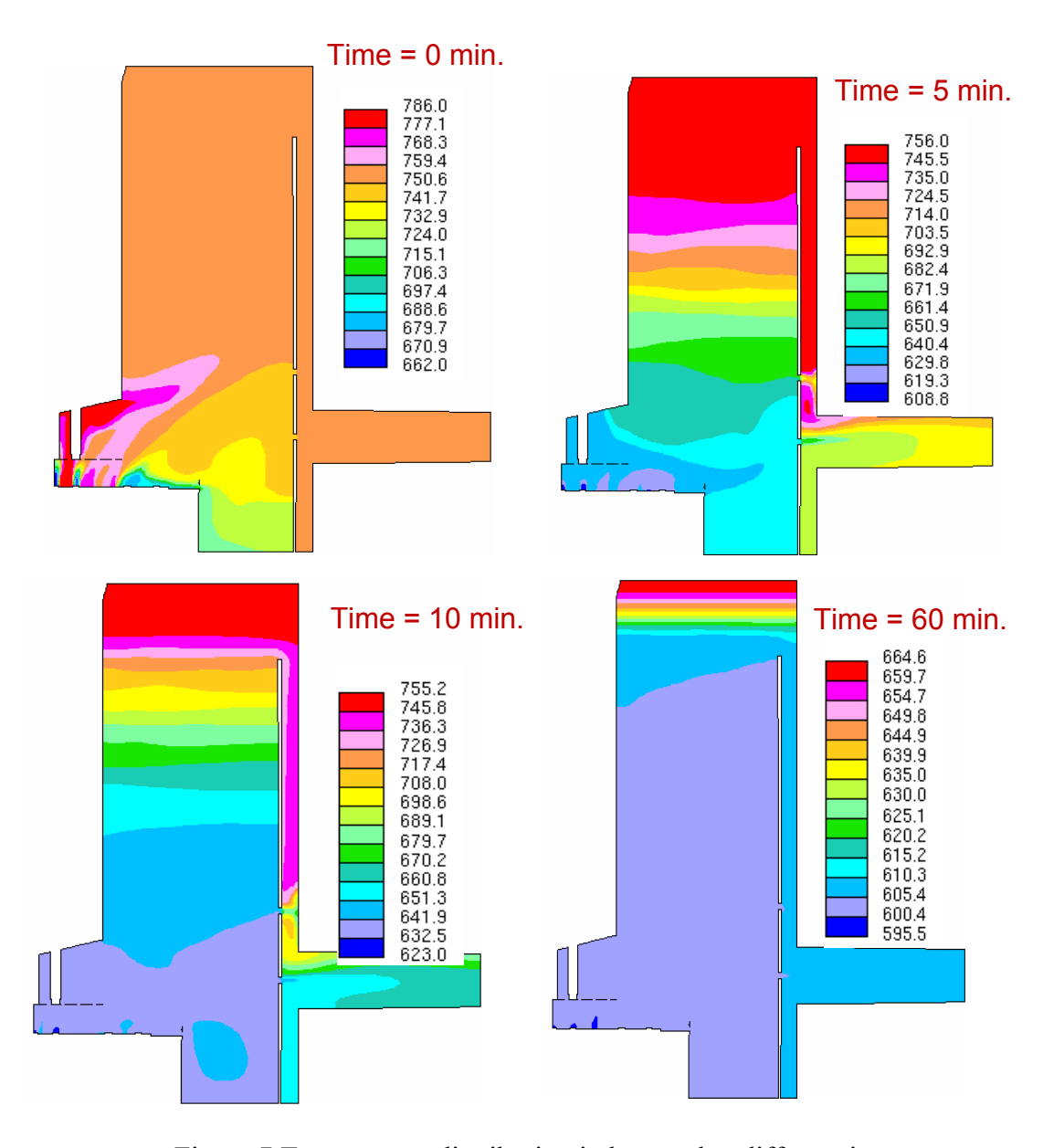


Figure 7 Temperature distribution in hot pool at different instants

3.4 Comparison with experimental data

The temperature along the thermocouple rack was measured during a planned trip of the reactor [10]. The comparison of simulation results is given in Fig. 8. At steady state, the numerical results compare reasonably well with the experimental data in the upper regions. However, in the lower part, the temperature predicted by CFD model is higher than the measured data. In order to check if this deviation is due to inadequate convergence, the errors in the continuity and energy equations were

reduced by one order, i.e., 10⁻⁶. But, no significant improvement in the prediction could be achieved. The other possible reason for the deviation is the boundary condition employed at the bottom region beyond core barrel. In the present simulation, an adiabatic boundary is assumed, while in reality there may be significant heat exchange between the hot and the cold pools. This aspect is being investigated in the future studies. During transient, temperatures in the bottom regions are well predicted, while there are significant deviations in the upper regions. Also, the stratification front in numerical simulation moves upward faster than the actual front. This may be due to possible inaccurate modelling of the holes in the inner barrel, which is further investigated as a part of the collaborative project.

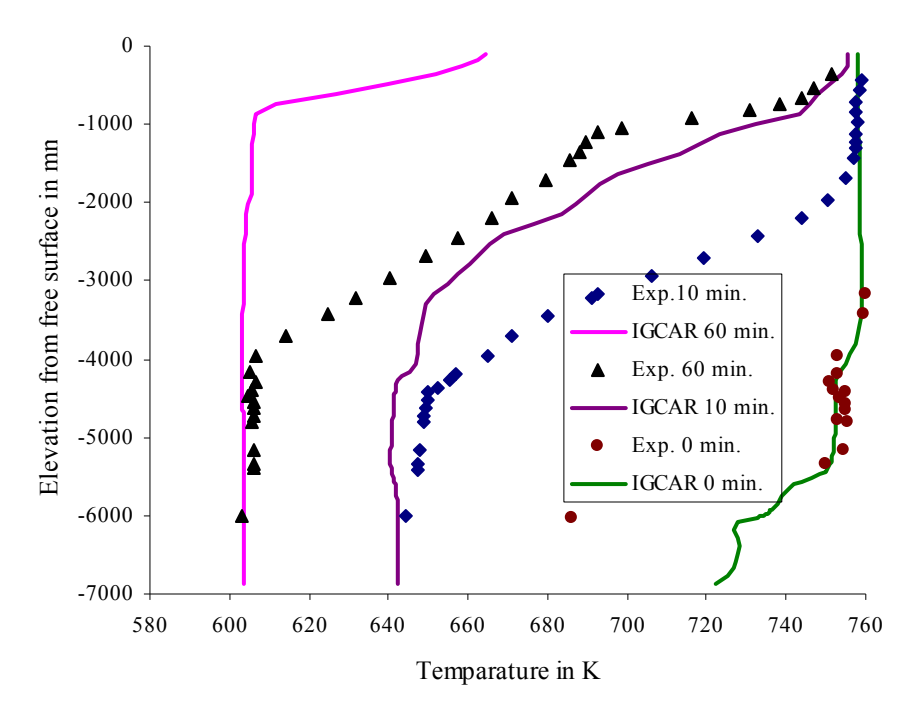


Figure 8 Comparison of temperature along thermocouple tree at various instances with experimental data

3.5 Effect of thermal capacity on sodium stratification

The effect of thermal capacity on thermal stratification of hot pool is also studied by accounting all the structures in contact with hot pool sodium. No significant changes in the flow patterns were observed between the benchmark model and the thermal capacity model. Temperature distribution along the thermocouple rack, predicted by the thermal capacity model is compared against that of the benchmark model in Fig. 9. From the plot it can be seen that the temperature at the thermocouple location are nearly same in both benchmark model and thermal capacity model.

3.6 Influence of turbulence model on predicting stratification

In order to see if the Reynolds Stress Turbulence Model (RSTM) has different predictive capability of thermal stratification, the transient simulation was carried out using this model for a duration of 3600 s. No appreciable change in the flow and temperature distributions in the pool were observed while employing the RSTM model. Temperature along the thermocouple tree, predicted by RSTM model is compared against that predicted by the standard high Reynolds number k-ε model in Fig, 10. The interface thermal gradient predicted by the RSTM model is less than that predicted by the k-ε model. The predicted gradient is closer to that measured in the plant. But the interface vanishes while in the tests, the interface persisted even after 1 h. This gives an impression that there may be

larger flow by-pass through the inner barrel holes than that predicted by the present model. Future works will be in this direction.

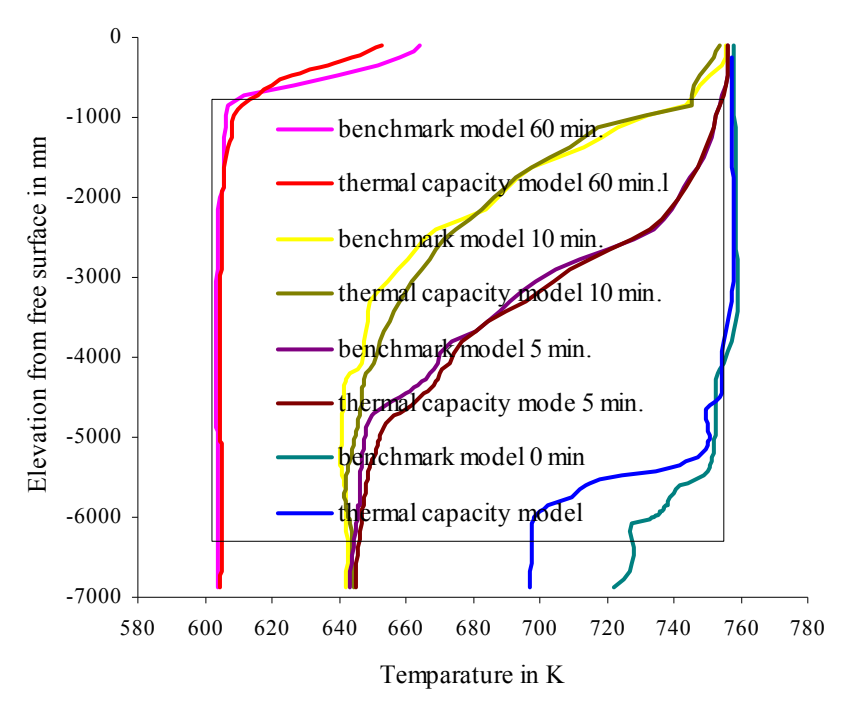


Figure 9 Comparison of temperature along thermocouple tree at various instances: Effect of thermal capacity of hot pool structures

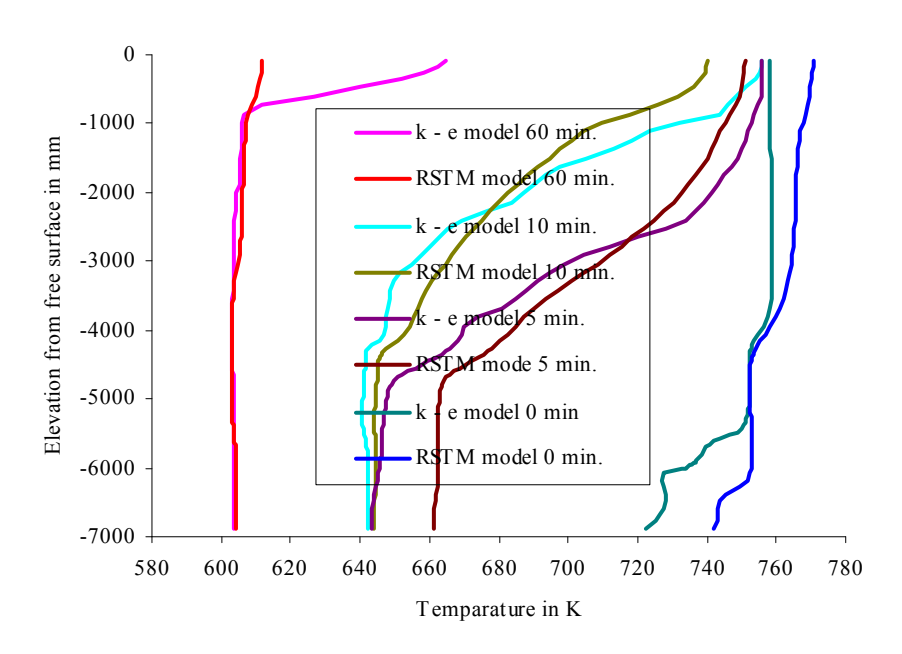


Figure 10 Comparison of temperature along thermocouple tree at various instances: Prediction of RSTM vs. k-ε model

4. Conclusions

Flow and temperature distributions in the hot pool of MONJU reactor, during the simulated event of reactor trip following a "Condenser vacuum low" signal have been simulated using CFD code STAR-CD. It is seen that there is stratification during initial steady state itself. Further the CFD simulation over-predicts the upward movement of stratification interface, when compared with the plant data. Further, the temperature gradient at the interface is sharper in numerical simulations than that in the measurements. Thermal capacity of hot pool structures is found to have insignificant effect on thermal stratification characteristics. No significant improvement in the prediction could be achieved by using the RSTM model.

5. References

- [1] Azarian, M., Astegiano, J.C., Tenchine, D., Lacroix, M., and Vidard, M., "Sodium thermal-hydraulics in the pool LMFBR primary vessel", Nuclear Engineering and Design, Vol. 124, pp. 417-430, 1990.
- [2] Francois, G., Azarian, G., Astegiano, J.C., Lacroix, C., Poet, G., "Assessment of Thermalhydraulic Characteristics of Primary Circuit", Nuclear Science and Engineering, Vol. 106, pp. 55-63, 1990.
- FBR Plant Technology Unit, "Data description for numerical analysis of sodium natural convection in the upper plenum of the MONJU reactor vessel", Advanced Nuclear System Research and Development Directorate, JAEA, Presented at the First (Kick-off) Research Coordination Meeting (RCM) of the IAEA-Coordinated Research Project (CRP) on, "Benchmark Analyses of Sodium Natural Convection in the Upper Plenum of the MONJU Reactor Vessel", IAEA Headquarters, Vienna. 22 24 September 2008.
- [4] FBR Plant Technology Unit, "Complementary descriptions for detailed boundary conditions", Advanced Nuclear System Research and Development Directorate, JAEA, Presented at the First (Kick-off) Research Coordination Meeting (RCM) of the IAEA-Coordinated Research Project (CRP) on, "Benchmark Analyses of Sodium Natural Convection in the Upper Plenum of the MONJU Reactor Vessel", IAEA Headquarters, Vienna, 22 24 September 2008.
- [5] Thermodynamic and Transport Properties of Sodium Liquid and Vapor" (ANL/RE-95/2).
- [6] CD adapco Group, 2005, STAR-CD, ver. 3.2, Computational Dynamics Limited.
- [7] W. F. Hughes and E. W. Gaylord, 1964, "Basic Equations of Engineering Science", McGraw-Hill, New York
- [8] B. E. Launder and D. B. Spalding, "The numerical computation of turbulent flows" Computer Methods in Applied Mechanics and Eng. Vol. 3, pp. 269-289, 1974.
- [9] Vincent Blin, Ulrich Bieder, Tanju Sofu, "Benchmark Analysis of Sodium Natural Convection in the Upper Plenum of the MONJU Reactor Vessel: Preparation of a simplified model for the Upper Core Structures", DEN/CAD/DER/SSTH/LMDL/NT/2009-105/A.
- [10] Shinji Yoshikawa and Masaki Minami, "Data description for the second Research Coordination Meeting of the IAEA Coordinated Research Project on Benchmark Analyses of Sodium Natural Convection in the Upper Plenum of the MONJU Reactor Vessel", IAEA Headquarters, Vienna22 24 September 2008.

* * *